Article:
Li, Chunqing and Hancock, Edwin R (2018) Vertex-Level Three-Dimensional Shape Deformability Measurement Based on Line Segment Advection. IET Computer Vision. ISSN: 1751-9632

https://doi.org/10.1049/iet-cvi.2017.0500

IET Journals
The Institution of Engineering and Technology

Vertex-Level Three-Dimensional Shape Deformability Measurement Based on Line Segment Advection

ISSN 1751-8644
doi: 0000000000
www.ietdl.org

Yuelong Li[1,2*], *Edwin R. Hancock*[3], *Zhitao Xiao*[4], *Lei Geng*[4], *Jun Wu*[4], *Fang Zhang*[4], *Chunqing Li*[1,2]

[1] *School of Computer Science and Software Engineering, Tianjin Polytechnic University, Tianjin 300387, P.R. China*
[2] *Tianjin Key Laboratory of Optoelectronic Detection Technology and System, Tianjin Polytechnic University, Tianjin 300387, P.R. China*
[3] *Department of Computer Science, University of York, York YO10 5GH, UK*
[4] *School of Electronics and Information Engineering, Tianjin Polytechnic University, Tianjin 300387, P.R. China*
* *E-mail: liyuelong@pku.edu.cn*

Abstract: The measurement to the intrinsic deformability of arbitrary small-scale subdivision of a shape is an interesting meanwhile valuable research topic. Such measurement can be directly utilized as a reliable criteria to partition object shape into small components and then assist in accurate shape modeling and description. Compared with single global shape modeling, through constructing subdivision-based complex shape description, the accuracy and flexibility of shape representation can be significantly improved. In this paper, we propose a line segment advection based vertex-level three-dimensional shape deformability measuring method. This measuring strategy can highlight the deformability characteristics of each shape part in any scale and size, at the same time, quantitatively describe them. The measurement is realized mainly based on the advection of line segments connecting neighboring shape mesh vertices. For 3D shapes, since the line segment of triangular mesh facet directly reflects the minimal neighborhood relationships and mesh microstructure, its advection can capture the finest details of shape deformability. Then, after transferring those information into neighboring vertices, a vertex-level shape deformability measurement can be acquired. Besides the measuring method, in order to demonstrate its value to shape partitioning and piecewise shape modeling, a straightforward shape partitioning method based on the proposed measurement is introduced as well, which is implemented through unsupervised clustering. Extensive experiments on three publicly available databases are conducted to verify the effectiveness of proposed methods.

1 Introduction

As a fundamental appearance characteristic, the surface shape of object has been a sustained focus of research in a number of cognate fields including computer vision, pattern recognition, image processing, and so forth [1]. The retrieval, correspondence, matching, and modeling of shapes are all popular research topics, which are of pivotal importance to higher level researches such as object recognition, activity analysis, and computer animation. In this paper, our main focus is the three-dimensional shape representation and modeling.

In the past few decades, many effective and well-designed shape modeling methods have been worked out [2]. EGI [3], Shape Distributions [4], 3D moments [5], and Polar-Fourier [6] explore the utilization of geometrical features in 3D shape representation. Structural models are introduced by approaches like MRG [7], ARG [8], and Skeleton [9]. The symmetry of object is incorporated into the approaches proposed by [10] and [11]. In addition, Spin-images [12] and Point Signatures [13] use the local parameters of object.

Linear modeling is a class of classical data representation approaches, which is commonly utilized in shape description. Generally, it is concise, computing efficient, and easily implemented. These advantages are quite important especially to complex three-dimensional shapes (the overall dimensionality of a 3D shape as a whole is usually tremendously higher compared with its 2D counterparts). That is why this class of techniques is still quite prevalent [14–23], even though many more accurate nonlinear modeling approaches have been worked out. One thing to be mentioned is that a majority of linear modeling techniques adopt Principal Component Analysis (PCA) [24] as a fundamental tool to realize linear shape representation.

However, the curse of representation accuracy is still a problem that has to be faced by linear shape models. This is an unavoidable challenge. Nonlinearly deformable to some extent is an intrinsic

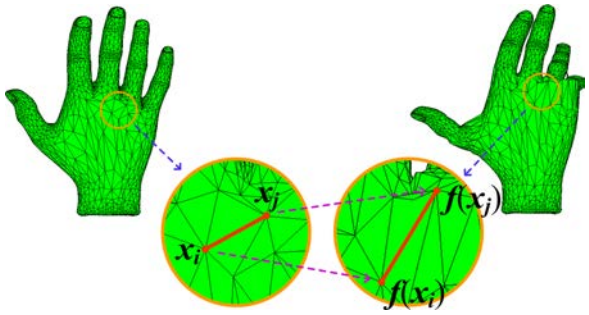

Fig. 1: A pair of corresponding line segments on two distinct shapes of a same right hand.

characteristic of a large amount of object surfaces, and clearly, linear models are unable to precisely describe this kind of intra variations. As to this problem, piecewise linear models or component-wise linear models may be an effective solution. These approaches decompose a whole shape model into a combination of several linear shape models specified for separate components, and actually offer a delicate trade-off between conciseness and accuracy. Without a doubt, an appropriate component partitioning strategy plays a vital role in this class of methods. In the past few years, the idea of piecewise linearity has been adopted by a number of modeling approaches [20, 25, 26], but a majority of them rely on manual component division, which directly degrades the degree of automation and robustness. Thus, in this paper, we want to discuss an automatic shape partitioning strategy.

Intuitively, a wise partitioning approach should throw sub-areas with similar deformability into the same component, so as to minimize the representation difficulties faced by each individual component model. In terms of 3D shapes, vertex is the minimum area

constituting unit. Hence, 3D shape partition can be described as a problem of vertex clustering. In this paper, we will introduce a vertex-level shape deformability measuring method, where the deformable ability of each vertex can be quantitatively evaluated and represented. Clearly, this measurement can be utilized to guide the procedure of shape partitioning, and elevate the opportunity of deforming similar vertices being clustered together.

The basic idea of the proposed method can be traced to particle advection, which is a newly developed technique to analyze and predict crowd scenes [27–29], where a lot of particles are overlaid on the first frame of analyzed videos and then advected sequentially. This concept is closely related with dynamical system. Through monitoring particle advection, the moving modes and rules of crowd can be clearly disclosed. Motivated by this technique, we will quantitatively evaluate small-scale shape deformability through the advection of tiny line segments in a bunch of kindred 3D shapes.

As shown in Fig. 1, in 3D shapes, the tiny line segments connecting neighboring vertices can directly reflect the finest shape structure. Hence, through measuring the variation patterns of these line segments, the overall deformability of shape in any small scale can be acquired. Then, after integrating and injecting this information into neighboring vertices, a vertex-level shape deformability measurement can be obtained. One thing to be mentioned is that, since line segment advection (LSA) has to be conducted on corresponding line segments (as demonstrated in Fig. 1), its source training set must be constituted by aligned shapes. With the impressive development of 3D shape acquisition devices and techniques in the past few decades, we believe this is not a tough prerequisite.

The effectiveness of this deformability measuring method has been examined both qualitatively and quantitatively on three publicly available 3D shape databases. Here, since the direct quantitative validation is hardly achieved, an indirect approach is worked out instead. It is done by evaluating the improvement to model reconstruction accuracy by introducing LSA based automatic shape partition into PCA based piecewise linear shape modeling.

To summarize, the main contributions of this paper are threefold:

1. A vertex-level 3D shape deformability measuring approach is introduced, which can concisely but clearly evaluate the deformability of arbitrary shape parts in any small scale. It is of great value to automatic piecewise shape modeling.
2. The idea of small-scale deformability guided shape partitioning is worked out.
3. An automatic shape component partitioning strategy is proposed, based on the deformability measurement worked out by LSA.

The remainder of this paper is organized as follows. Section 2 introduces the LSA based 3D shape deformability measuring method in detail. Then, the method of LSA driving automatic shape partitioning is discussed in Section 3. Experiments are conducted in Section 4. Section 5 concludes this paper and explores potential directions for future works.

2 LSA Based 3D Shape Deformability Measurement

It is well known that a single global linear model can not precisely represent nonrigid deformable shapes. But if a overall deformable shape can be divided into a series of components, and then those components are linearly modeled separately, with no doubts, the representation difficulties will be evidently reduced. It is this idea that underlies piecewise linear shape modeling. However, piecewise modeling introduces an extra problem, how to partition a given shape automatically. Since the difficulties faced by modeling techniques are directly related with intrinsic shape deformability, a wise shape partitioning scheme should take into account this information as a main gist, and throw the sub-areas with similar deformability into a same shape partition. In this section, we will give a detailed introduction about the linear segment advection based vertex-level shape deformability measuring method. Since vertex is the minimum 3D shape constituting element, this measurement can effectively reflect the deformability of any scale shape areas.

Suppose $\boldsymbol{x}_i$ and $\boldsymbol{x}_j$ represent two arbitrary neighboring vertices on a 3D shape $\boldsymbol{s}_0$, and there is a transformation $\boldsymbol{f}_0^t : \mathbb{R}^3 \rightarrow \mathbb{R}^3$ that can transfer vertices of shape $\boldsymbol{s}_0$ onto those of shape $\boldsymbol{s}_t$, in a manner similar to that illustrated in Fig. 1. Here $t = 1, 2, \ldots, N$ denotes shape index. All training shapes are required to have rigorous vertex and triangulation correspondence.

In 3D shapes, the line segments connecting shape vertices constitute the overall topology of shape, and determine the granularity and resolution of the represented surface. Thus, they can directly reflect the characteristics of the tiniest 3D shape structure. Any small-scale shape pose deformation will cause (and actually is determined by) the variance of corresponding line segments. According to this property, our deformability measuring strategy is achieved mainly based on the evaluation to the variance of corresponding line segments among shapes, pairs by pairs sequentially, namely the concept of line segment advection. Here, to obtain a competent deformability measurement, the training set should be constructed by shapes with various poses while rigorously aligned. In order to precisely represent line segment variance, we first explored an indicator based on the concept of partial differential, namely,

$$\frac{\partial \boldsymbol{f}_0^t(\boldsymbol{x})}{\partial \boldsymbol{x}} = \lim_{(\boldsymbol{x}_i - \boldsymbol{x}_j) \rightarrow \mathbf{0}} \frac{\boldsymbol{f}_0^t(\boldsymbol{x}_i) - \boldsymbol{f}_0^t(\boldsymbol{x}_j)}{\boldsymbol{x}_i - \boldsymbol{x}_j}. \tag{1}$$

Clearly, it can be observed that, in the right part of this equation, the numerator actually corresponds to a line segment on shape $\boldsymbol{s}_t$, while the denominator is its counterpart in shape $\boldsymbol{s}_0$. Hence, $\frac{\partial \boldsymbol{f}_0^t(\boldsymbol{x})}{\partial \boldsymbol{x}}$ actually reflects the advection of line segments between shape $\boldsymbol{s}_t$ and $\boldsymbol{s}_0$. This indicator has obvious theoretical foundation. Since the limit operation pushes $(\boldsymbol{x}_i - \boldsymbol{x}_j)$ infinitely approaching $\mathbf{0}$, which means the minimum shape line segment can be covered, the finest grained shape deformations can be reflected by this indicator.

Because both $\boldsymbol{f}_0^t(\boldsymbol{x})$ and $\boldsymbol{x}$ are vectors, $\frac{\partial \boldsymbol{f}_0^t(\boldsymbol{x})}{\partial \boldsymbol{x}}$ is in fact a 3×3 Jacobian matrix,

$$\frac{\partial \boldsymbol{f}_0^t(\boldsymbol{x})}{\partial \boldsymbol{x}} = \begin{pmatrix} \frac{\partial f_1}{\partial x_1} & \frac{\partial f_1}{\partial x_2} & \frac{\partial f_1}{\partial x_3} \\ \frac{\partial f_2}{\partial x_1} & \frac{\partial f_2}{\partial x_2} & \frac{\partial f_2}{\partial x_3} \\ \frac{\partial f_3}{\partial x_1} & \frac{\partial f_3}{\partial x_2} & \frac{\partial f_3}{\partial x_3} \end{pmatrix}. \tag{2}$$

Though this is not a scalar representation, the first eigenvalue of $\frac{\partial \boldsymbol{f}_0^t(\boldsymbol{x})}{\partial \boldsymbol{x}}^T \cdot \frac{\partial \boldsymbol{f}_0^t(\boldsymbol{x})}{\partial \boldsymbol{x}}$ or the simple matrix determinant $|\frac{\partial \boldsymbol{f}_0^t(\boldsymbol{x})}{\partial \boldsymbol{x}}|$ can be used, if a scalar measurement is preferred. Hence, $\frac{\partial \boldsymbol{f}_0^t(\boldsymbol{x})}{\partial \boldsymbol{x}}$ seems to be a competent shape deformability measurement. But when try to actually calculate it, things are different.

It should be noticed that according to the right part of Eq. (2), the "actual" value of $\frac{\partial \boldsymbol{f}_0^t(\boldsymbol{x})}{\partial \boldsymbol{x}}$ that can be obtained in practice does not reflect the characteristics of line segments which actually constitute 3D shapes. That is because since as to discrete 3D shape data, the accurate calculation is unrealizable, generally each entry of this Jacobian matrix can only be worked out through coordinate grid based approximation. This is similar with the mechanism of the calculation of 2D image gradient ($\frac{\partial I}{\partial \boldsymbol{x}}$), where since the analytical function expression of image dose not actually exist (as that of $\boldsymbol{f}(\boldsymbol{x})$ does), grid-level approximation methods (such as Sobel, Prewitt, and Roberts) have to be utilized. During these approximation, for example, suppose $\boldsymbol{x} = [0, 0]^T$, the value of $\frac{\partial I}{\partial \boldsymbol{x}}$ can be worked out only based on five neighboring (grid-level) pixels, namely, $(0, 0)^T$,$(-1, 0)^T$,$(1, 0)^T$,$(0, -1)^T$, and $(0, 1)^T$. Clearly, in this process, none of actual line segments in image $I(\boldsymbol{x})$ has been considered (because line segments are on vertex-level while the calculation is on grid-level). Therefore, it can be deduced that in practical application, the value of $\frac{\partial \boldsymbol{f}_0^t(\boldsymbol{x})}{\partial \boldsymbol{x}}$ can not actually reflect the variance of shape line segments, which is the first priority for designing a deformability measuring method. Thus, due to the constraints incurred by practical calculation, $\frac{\partial \boldsymbol{f}_0^t(\boldsymbol{x})}{\partial \boldsymbol{x}}$ is not a qualified indicator, and other more appropriate alternatives must be worked out.

Motivated by the right part of Eq. (1), we believe direct line segment comparison may be a good indicator. For one thing, it

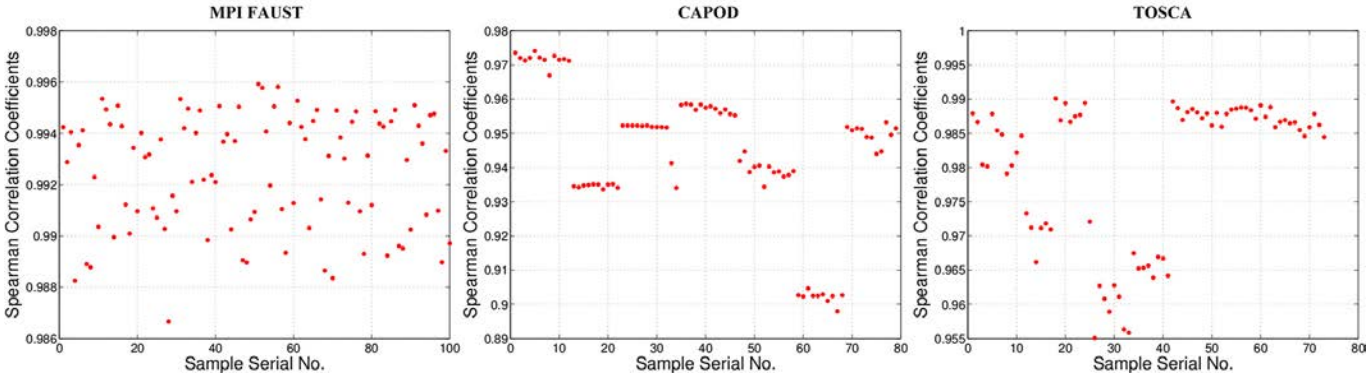

Fig. 2: The Spearman's rank correlation coefficients between triangle area and corresponding edge length on 3D shapes of three data sets which the following experiments are carried on. Here each coefficient (which corresponds to a red point on the figures) is calculated based on an array formed by all triangles on a sample shape.

can straightforward reflect small-scale shape variation. For another, as represented by Eq. (1), it directly relates with the definition of $\frac{\partial \boldsymbol{f}_0^t(\boldsymbol{x})}{\partial \boldsymbol{x}}$, an easily understood subtle shape deformability descriptor (as to its physical meaning), which has been introduced in the beginning of this section. In addition, if we take a closer look at Eq. (1), it can be deduced that in terms of 3D shapes, the actually existing $(\boldsymbol{x}_i - \boldsymbol{x}_j)$ that approach zero are exactly the line segments starting from $\boldsymbol{x}_i$ (let $\frac{\partial \boldsymbol{f}_0^t(\boldsymbol{x}_i)}{\partial \boldsymbol{x}}$ be considered). Clearly, this fact further reinforces the relationships between actual line segments of 3D shapes and partial differential of shape transformation, and implies the effectiveness of line segment based shape deformability measuring method from another view.

As to the quantitative measurement of line segment comparison, it is well known that there are two approaches, subtraction and division. Here, we choose the former, and specifically, it is defined as,

$$\Delta_0^t(\boldsymbol{x}_i, \boldsymbol{x}_j) = \boldsymbol{f}_0^t(\boldsymbol{x}_i) - \boldsymbol{f}_0^t(\boldsymbol{x}_j) - (\boldsymbol{x}_i - \boldsymbol{x}_j), \tag{3}$$

where the subscript 0 and superscript t represent this is a measurement to the difference of line segment $(\boldsymbol{x}_i - \boldsymbol{x}_j)$ on shape 0 and t.

Here, besides higher computation efficiency, the subtraction representor is selected mainly because it reflects the absolute difference while the division operation provides a normalized difference measurement. As to the topic of shape deformability measurement, the absolute variance of line segment is a notable factor. The underlying reason is that the length of line segment directly correlates with its significance in 3D shapes. It is well known that in 3D shapes, relatively bigger triangles are generally more important than their smaller counterparts, because they occupy larger area of shape surface. On the other hand, since during triangulation, plump acute triangles are evidently preferred (Note: as to the representation of 3D shape surface, plump acute triangles are much more advantageous than flat obtuse triangles, and hence triangulation algorithms generally intentionally select the former and avoid the latter [30].), in 3D shapes, line segment length is generally strongly related with the area of corresponding triangle. To demonstrate this relevance, Fig. 2 summarizes the Spearman's rank correlation coefficients between line segment length and corresponding triangle area on 3D shapes of three data sets. According to the figure, all Spearman coefficients have values approaching 1, which means evident monotonic relationship. Hence, it can be deduced that the influence to shape structure caused by the variance of longer line segments and shorter ones at the same rate will be distinct. For instance, 10% of the variance of $\|\boldsymbol{x}_i - \boldsymbol{x}_j\|$ at length 10 is 1, while its counterpart at length 1 is only 0.1. However, it is totally the same to a division operation based measurement. According to this fact, it is clear that an absolute line segment difference based indicator is preferred as to the task of shape deformability measurement.

As to the specific calculation of overall shape deformability, in order to maximize the deformability information conveyed by all available training shapes, the process of line segment advection will be conducted on each shape one by one, and thus, the variance evaluator $\Delta_0^t(\boldsymbol{x}_i, \boldsymbol{x}_j)$ should be rigorously represented as $\Delta_{t-1}^t(\boldsymbol{x}_i, \boldsymbol{x}_j)(t = 1, 2, ..., N)$. Fig. 3 demonstrates an example of line segment advection procedure.

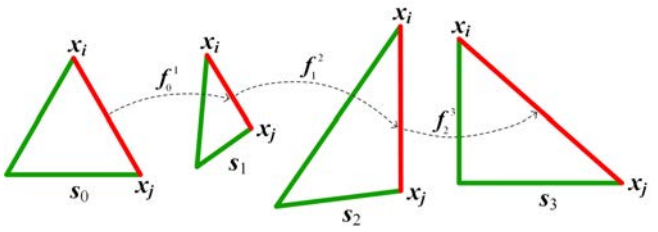

Fig. 3: A demonstration of line segment advection among triangular shapes.

On the other side, as we have mentioned above, since vertex is the most fundamental 3D shape constituting element, a vertex-level deformability measuring method is favorite to the task of shape partitioning. As to the deformability description of a vertex, it can be deduced from the right part of Eq. (1) that the line segments exact connecting with this vertex are the most vital factors, because they are the only actually existing $(\boldsymbol{x}_i - \boldsymbol{x}_j)$ that approach but not equal to zero. Motivated by this idea, our vertex-level deformability indicator is defined as the average of all deformability measurements of the line segments which directly connect with the vertex, namely,

$$\boldsymbol{c}_{t-1}^t(\boldsymbol{x}_i) = \frac{1}{M_i} \sum_{\boldsymbol{x}_j \in U(\boldsymbol{x}_i)} \Delta_{t-1}^t(\boldsymbol{x}_i, \boldsymbol{x}_j), \tag{4}$$

where $U(\boldsymbol{x}_i)$ denotes the set of all vertices that are actually connected with vertex $\boldsymbol{x}_i$, which means there is a line segment between $\boldsymbol{x}_i$ and each element of $U(\boldsymbol{x}_i)$, and M_i is the size of $U(\boldsymbol{x}_i)$.

Correspondingly, the general vertex-level deformability measurement obtained from all training shapes is defined as the mean of all $\boldsymbol{c}_{t-1}^t(\boldsymbol{x}_i)$, namely,

$$\boldsymbol{c}(\boldsymbol{x}_i) = \frac{1}{N} \sum_{t=1}^{N} \boldsymbol{c}_{t-1}^t(\boldsymbol{x}_i). \tag{5}$$

It can be observed that since the variance of all shape line segments are involved and evaluated in this measurement, it can effectively reflect the characteristics of overall shape deformability in any small scale. Hence, it should be a reliable indicator to assist automatic 3D shape partitioning.

3 A LSA Measurement Assisted Shape Partitioning Approach

In the previous section, we have introduced a vertex-level 3D shape deformability measuring method, which is mainly driven by line segment advection. Since vertex is the minimum constituting element of 3D shape, this measurement can effectively reflect shape deformability in any small scale. Clearly, when it is used to assist the process of shape partitioning, vertices that have similar deformability may have more opportunities to be thrown into a same partition, and hence a more accurate and concise piecewise shape model can be constructed.

In this section, we will introduce a straightforward shape partitioning approach with LSA embedded, to demonstrate how to utilize the proposed deformability measuring method as an example. On the other side, since the direct quantitative evaluation to the performance of LSA is hardly achieved, this approach can be used to indirectly exhibit its effectiveness as well. But, it should be noted that this approach is only a simple and intuitional application of LSA for demonstration purpose, rather than an elaborately designed framework to achieve the highest accuracy. Here, because the proposed partitioning method will be utilized to verify the quantitative performance of LSA, we haven't designed a highly integrated powerful approach to avoid the potential confusion about who really contributes the performance, LSA or any other integrated approaches? Hence, when LSA is used in real partitioning applications, we suggest more subtle shape partitioning approaches should be specially designed.

The core idea of this shape partitioning approach is to evidently utilize LSA. According to this idea, we design a method mainly based on the classic unsupervised clustering framework, where the deformability indicator $\boldsymbol{c}(\boldsymbol{x}_i)$ is directly used as part of the feature vector. Then, considering if the clustering algorithm only relies on the deformability measurement, a large number of neighboring vertices may be over-segmented, vertex coordinate is also enrolled as part of the clustering feature. In a word, the overall clustering feature vector $\boldsymbol{w}(\boldsymbol{x}_i)$ can be represented as,

$$\boldsymbol{w}(\boldsymbol{x}_i) = [\boldsymbol{x}_i; \alpha(\boldsymbol{x}_i) \cdot \boldsymbol{c}(\boldsymbol{x}_i)], \tag{6}$$

where $\alpha(\boldsymbol{x}_i)$ is a positive real coefficient that balances the significance of vertex coordinate and LSA measurement. Its specific expression is,

$$\alpha(\boldsymbol{x}_i) = \rho \frac{\|\boldsymbol{x}_i\|}{\|\boldsymbol{c}(\boldsymbol{x}_i)\|}, \quad \rho > 0. \tag{7}$$

Here, it can be observed that by introducing the coefficient $\alpha(\boldsymbol{x}_i)$, the first and second part of $\boldsymbol{w}(\boldsymbol{x}_i)$ can be adjusted to comparable magnitudes, so that both parts can really play a role during shape partitioning.

The positive real coefficient ρ is a parameter required to be determined beforehand. It is well known that accurately calculating the optimal parameter value is usually time consuming, moreover, a robust method should not be oversensitive to slight parameter value variance. Thus, in specific implementation, a fixed interval sampling based candidate parameter value set is first constructed. Then, the specific value will be picked up from this set through cross validation. Though this strategy can not guarantee to acquire the optimal ρ, if the algorithm is moderately robust to parameter value choice, it will not incur significant performance degradation.

The algorithm is specifically implemented based on the k-means clustering framework [31]. It is well known that k-means is a classic clustering technique with quite straightforward and easily understood intrinsic structure. Due to its simpleness, we believe the effectiveness of the proposed LSA measurement can be clearly verified.

4 Experiments

To validate the effectiveness of LSA and quantitatively evaluate its capability, in this section we will conduct extensive experiments on three publicly available 3D shape databases, namely, MPI FAUST [32], CAPOD [33], and TOSCA [34]. Fig. 4 shows a few samples of experimental data.

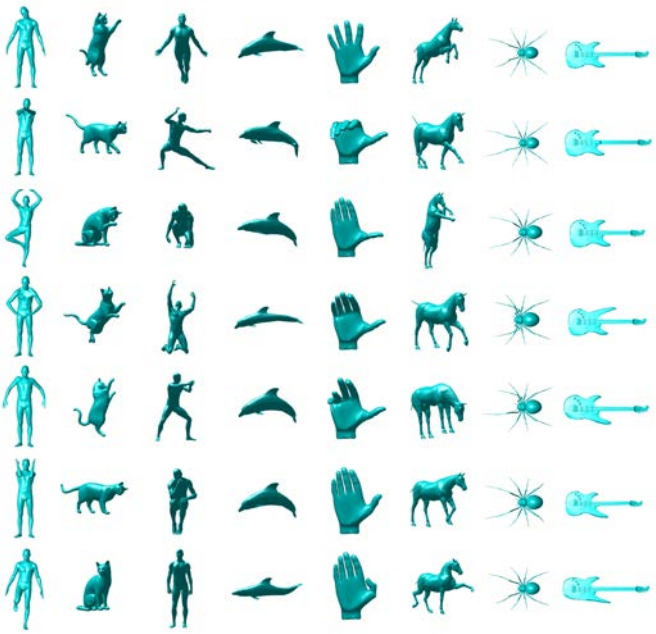

Fig. 4: Samples of experimental data. Fig. 5 will demonstrate the performance of LSA measurement when using all the 7 shapes of each column here as the input.

The MPI FAUST database is comprised by a series of human body shapes belonging to 10 subjects in diverse poses. The shapes are triangulated and each contains 6890 vertices. Since all shapes of the test subset of this database are not aligned, which is a fundamental prerequisite of advection based method, our experiments are conducted on its training subset that contains 100 shapes (10 for each subject).

The CAPOD database contains shapes of 15 classes of generic objects with various poses. Our experiments are conducted on 74 shapes of 7 classes (the others are discarded because they do not have uniform shape compositions, for instance some shapes of the piano class contain a stool while others do not). It should be noticed that the shape size in this database is relatively small: its number of vertices ranges from 346 to 3620.

The TOSCA database is composed of high resolution nonrigid shapes. It includes 9 distinct object classes, such as cat, dog, horse, and so forth. Since among them, two classes have less than 5 samples (too small training set can not sufficiently expose the underlying deformability), we utilize the remain 7 classes to construct the experimental data set. The shape resolution is from 15768 to 52565 vertices, much denser than the other two databases.

4.1 Qualitative Experiments

Fig. 5 demonstrates the qualitative performance of LSA, where each column of Fig. 4 is used as the training data respectively, and the corresponding output is shown on a neutral pose shape. It can be observed on the first row of the figure that LSA is able to appropriately reflect small-scale shape deformability: the shape parts corresponding to evident surface deformations are all marked out by brighter colors (which means they have higher LSA values), such as the arm, leg, and shoulder of body, the tail of cat, the head and tail of dolphin, the finger of hand, the feet of spider, and the neck and shoulder of guitar. Hence, it can be deduced that LSA measurement should be helpful to realize deformability oriented shape partitioning.

The second row of Fig. 5 shows the performance of the LSA assisted shape partitioning method introduced in Section 3. As demonstrated by the subfigures of the 1st, 2ed, 3rd, and 6th column,

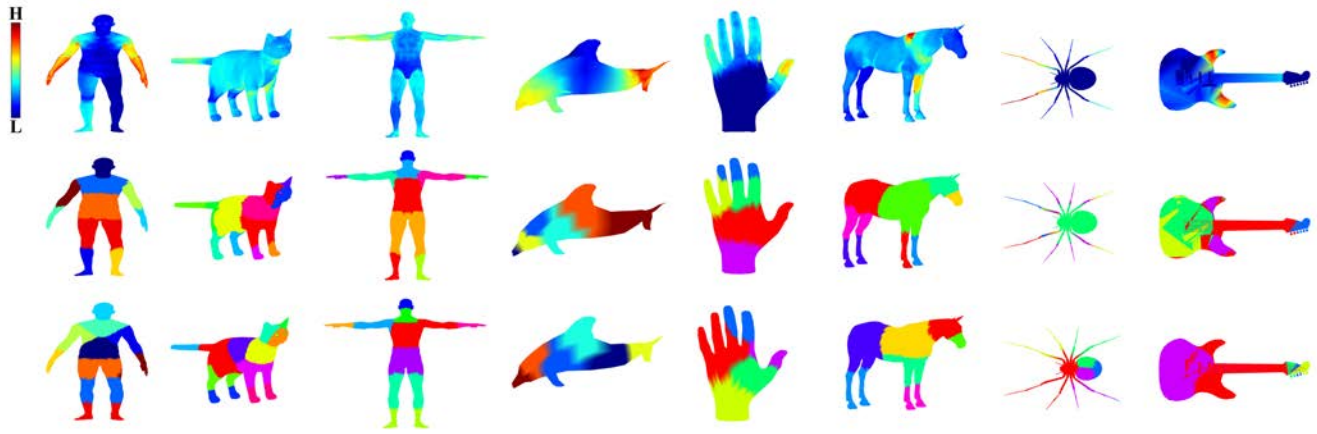

Fig. 5: The LSA based vertex-level shape deformability measurement learned from each column of Fig. 4, and the corresponding shape partitioning output. The first row is the norm of LSA measurement $\boldsymbol{c}(\boldsymbol{x}_i)$. The second row shows the shape partitions worked out by the approach introduced in Section 3. The third row is comprised by the partitions acquired only based on coordinate feature.

all legs of human, cat, and the front legs of horse are divided into different components (represented by distinct colors). Through looking up corresponding training shapes shown in Fig. 4, it can be deduced that this phenomenon is an appropriate reflection to the deformation patterns of training shapes, e.g., in the 1st column, the deformation mode of the left shank is evidently different with that of the right. On the other side, in the last column, the right bottom part of guitar is specifically divided out, and it can be observed from corresponding training shapes that this part indeed varies with unique characteristics compared with other shape parts. Clearly, throwing these unique deformable parts into extra components can effectively reduce the diversity of interior deformability, and hence can improve the accuracy of corresponding piecewise shape modeling. Comparatively, the partitions shown in the third row, namely the output worked out without the assistance of LSA, can not reflect this kind of emphasis on shape deformability.

In addition, since deformability is inherently correlated with object structure (vertices belonging to a same genuine object component generally have more opportunities to share similar deformability), it can be observed that LSA also brings other extra improvements and promotes the overall partitioning performance. For example, in the 1st column, LSA partitioning successfully locates upper arms; in the 3rd column, both hands are accurately segmented out; in the 5th column, the intactness of palm is reserved, while the varying patterns of fingers are effectively reflected, and similar circumstance can be observed on the partition of spider (the 7th column) as well.

4.2 Quantitative Experiments

In this paper, the quantitative verification experiments are indirectly conducted through shape partitioning. As to partition algorithm, since component number is a relatively subjective configuration and hardly predetermined, we choose to exhaustively experiment the situations ranging from 3 to 20 components. Each experiment is repeated 10 times with randomly selected training and evaluating samples. In addition, since according to Eq. (5), the value of $\boldsymbol{c}(\boldsymbol{x}_i)$ is related with the advection sequence (as exampled in Fig. 3), the training shape permutation order will be determined randomly as well.

Table 1 demonstrates the average SD (standard deviation) of LSA measurement within each shape partition of the divided shapes on the three data sets. This is actually an evaluation to the similarity of interior shape deformability within each shape partition. It can be observed that compared with undivided shapes (Global), piecewise shapes generally have much better interior deformability similarity, which means the representation difficulties faced by modeling techniques will be evidently reduced. Moreover, according to the table, it is clear that compared with coordinate clustering (Coordinate), our approach can consistently further improve this similarity.

In order to quantitatively evaluate the performance of LSA in assisting piecewise shape modeling, we will further inspect the representation/reconstruction accuracy. This series of experiments are implemented through commonly utilized PCA linear shape modeling, i.e.,

$$\boldsymbol{s} = \bar{\boldsymbol{s}} + \boldsymbol{P}\boldsymbol{b}, \tag{8}$$

where a shape $\boldsymbol{s}$ is described by the sum of the mean shape $\bar{\boldsymbol{s}}$ and the multiplication of eigenvector matrix $\boldsymbol{P}$ and model coefficient vector $\boldsymbol{b}$. The representation accuracy is evaluated through ℓ_2-norm minimization based shape reconstruction error, namely,

$$e = \left\| \boldsymbol{s} - [\bar{\boldsymbol{s}} + \boldsymbol{P}\boldsymbol{P}^T(\boldsymbol{s} - \bar{\boldsymbol{s}})] \right\|_2. \tag{9}$$

During piecewise shape modeling, there will be an individual PCA model for each separate shape partition, which means the representation vector and following reconstructed shape are calculated on each partition independently.

For comparison, we also conduct experiments with only vertex coordinates as the clustering feature, and when assisted by the norm of LSA (rather than the LSA vector). As demonstrated in Fig. 5, the norm of LSA can be utilized as a measurement to shape deformability as well.

On the MPI FAUST data set, there are 10 shapes for each subject. The experiments are carried out based on leave-one-out training and evaluating configuration, i.e., 9 training samples and 1 evaluating sample. The average reconstruction errors under different number of partitions are summarized in Fig. 6. It shows LSA stably improves the reconstruction errors under every shape partitioning assignment. Specifically, the LSA vector method achieves average 15.41% accuracy improvement over coordinate only clustering, while LSA norm improves 15.31%.

The CAPOD database contains many similar shapes and their deformation patterns are relatively simple. As a result, the leave-one-out configuration could easily lead to approximate zero reconstruction errors, which makes this series of experiments trivial. To overcome this flaw, we reduce the number of training samples to 7. The overall experimental performance is shown in Fig. 7. Compared with the performance on the MPI FAUST data set, here, LSA vector is evidently better than LSA norm. In detail, the advantage of LSA vector to sole coordinate is 35.71%, while that of LSA norm is 29.57%.

In experiments on the high resolution TOSCA database, the number of training samples has to be reduced to 5 to avoid running out of memory in our hardware platform (Intel i5 2.4 GHz and 6 GB memory). The reconstruction errors are demonstrated in Fig. 8. It can be observed that the performance is similar to that obtained on the other two data sets. The specific average promotion of LSA vector to coordinate only is 24.32%, and that of LSA norm is 12.46%.

Table 1 The Average SD of LSA Measurement within Each Shape Partition of the Divided Shapes.

Database	Global	Clustering Feature	Part Number 3	4	5	6	7	8	9	10	11	12	13	14	15	16	17	18	19	20
MPI FAUST	0.0067	Coordinate	0.0064	0.0062	0.0057	0.0057	0.0056	0.0053	0.0053	0.0052	0.0050	0.0048	0.0046	0.0044	0.0042	0.0040	0.0039	0.0039	0.0039	0.0037
		LSA+Coordinate	**0.0062**	**0.0059**	**0.0056**	**0.0054**	**0.0053**	**0.0051**	**0.0049**	**0.0046**	**0.0043**	**0.0043**	**0.0042**	**0.0040**	**0.0039**	**0.0038**	**0.0038**	**0.0037**	**0.0036**	**0.0036**
CAPOD	0.0557	Coordinate	**0.0483**	**0.0475**	0.0464	0.0442	0.0425	0.0417	0.0407	0.0405	0.0400	0.0392	0.0389	0.0376	0.0378	0.0374	0.0365	0.0368	0.0374	0.0372
		LSA+Coordinate	0.0492	0.0477	**0.0462**	**0.0437**	**0.0415**	**0.0415**	**0.0397**	**0.0390**	**0.0388**	**0.0387**	**0.0380**	**0.0363**	**0.0355**	**0.0365**	**0.0355**	**0.0356**	**0.0350**	**0.0346**
TOSCA	0.2408	Coordinate	0.2005	0.2013	0.1898	**0.1710**	0.1705	0.1560	0.1498	0.1518	0.1463	0.1443	0.1467	0.1458	0.1402	0.1371	0.1364	0.1330	0.1318	0.1320
		LSA+Coordinate	**0.1995**	**0.1919**	**0.1885**	0.1717	**0.1583**	**0.1510**	**0.1437**	**0.1430**	**0.1381**	**0.1394**	**0.1377**	**0.1285**	**0.1353**	**0.1315**	**0.1259**	**0.1268**	**0.1223**	**0.1244**

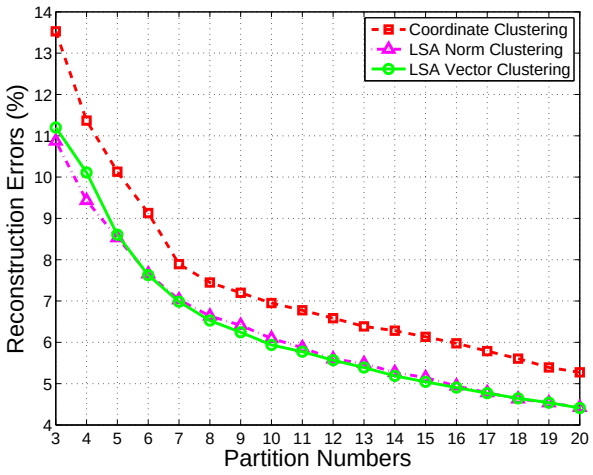

Fig. 6: The average shape reconstruction errors on the MPI FAUST data set.

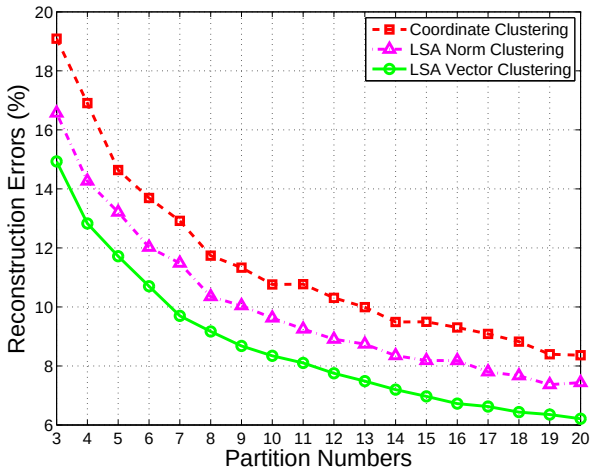

Fig. 8: The average shape reconstruction errors on the TOSCA data set.

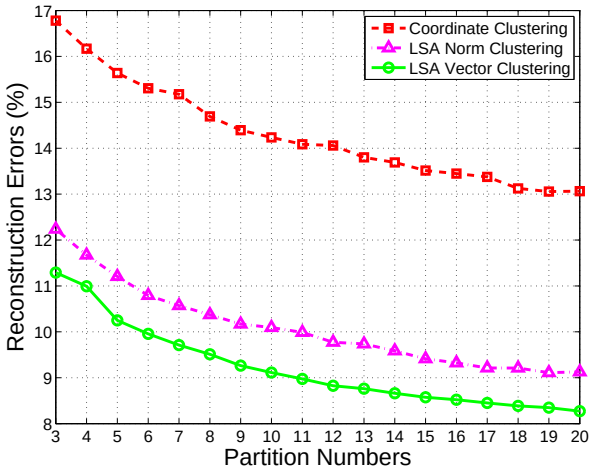

Fig. 7: The average shape reconstruction errors on the CAPOD data set.

In summary, according to the experimental performance on these three data sets, the proposed LSA measurement can faithfully reflect the characteristics of small-scale shape deformation, and effectively improve the accuracy of representing shape with piecewise shape models.

5 Conclusions and Future Works

In this paper, we have introduced an easily implemented vertex-level 3D shape deformability measuring method. By advecting and monitoring line segments, it can directly reflect small-scale deformability within the whole shape. It is of great value to the design of deformation centered shape partitioning method, and can evidently improve piecewise shape modeling performance. Through introducing this measurement into shape partitioning, vertices that have similar deformability characteristics will have more opportunities to be thrown into a same division, and therefore the complexity of deformation contained in each shape partition can be effectively reduced. Unique to the method is that it allows piecewise linear models to accurately describe more deformable complicated shapes, and significantly improves the representational compactness.

In this paper, we have qualitatively and quantitatively validated the effectiveness of LSA based deformability measurement. In the near future, we will advance this research in three directions. First, we will try to design an integrated powerful partitioning strategy to pursue the maximum representation accuracy promotion. Second, static shape structure characteristics, such as the curvature, will be incorporated with the proposed approach to further improve shape partitioning performance. Since structure feature is directly related with genuine shape component composition, this kind of combination may be helpful to keep the integrity of acquired shape parts, as to physical meaning. Third, other small-scale sub-structure advection based approaches will be explored, such as triangle.

6 Acknowledgments

This work was supported by the National Natural Science Foundation of China (Nos. 61771340, 61302127, 11326198, 61601325, 51378350), the China Postdoctoral Science Foundation (No. 2015M570228), the Opening Foundation of Tianjin Key Laboratory of Intelligence Computing and Novel Software Technology, the International Fostering Plan of Selected Excellent Postdoctors Subsidized by Tianjin City (2015), the Tianjin Research Program of Application Foundation and Advanced Technology (No.15JCYBJC16600), and the Textile Industry Association Applied Basic Research Program of China (No. J201509). Thanks for the academic visiting support of the China Scholarship Council.

7 References

1 R. Szeliski, Computer Vision: Algorithms and Applications, London: Springer-Verlag, 2010.
2 D. Frejlichowski, Three-dimensional object representation based on 2D UNL-Fourier shape descriptor, in: International Conference Image Analysis and Recognition, 2013, pp. 389–396.
3 B. K. P. Horn, Extended gaussian images, Proceedings of the IEEE 72 (12) (1984) 1671–1686.

4 R. Osada, T. Funkhouser, B. Chazelle, D. Dobkin, Matching 3D models with shape distributions, in: Proceedings of International Conference on Shape Modeling and Applications, 2001, pp. 154–166.
5 M. Novotni, R. Klein, Shape retrieval using 3D Zernike descriptors, Computer-Aided Design 36 (11) (2004) 1047–1062.
6 D. Frejlichowski, A three-dimensional shape description algorithm based on Polar-Fourier transform for 3D model retrieval, Image Analysis (2011) 457–466.
7 M. Hilaga, Y. Shinagawa, T. Kohmura, T. L. Kunii, Topology matching for fully automatic similarity estimation of 3D shapes, in: Proceedings of the 28th Annual Conference on Computer Graphics and Interactive Techniques, 2001, pp. 203–212.
8 T. Tung, F. Schmitt, Augmented reeb graphs for content-based retrieval of 3D mesh models, in: Proceedings of Shape Modeling Applications, 2004, pp. 157–166.
9 H. Sundar, D. Silver, N. Gagvani, S. Dickinson, Skeleton based shape matching and retrieval, in: Proceedings of Shape Modeling International, 2003, pp. 130–139.
10 M. Kazhdan, B. Chazelle, D. Dobkin, T. Funkhouser, S. Rusinkiewicz, A reflective symmetry descriptor for 3D models, Algorithmica 38 (1) (2004) 201–225.
11 M. Kazhdan, T. Funkhouser, S. Rusinkiewicz, Symmetry descriptors and 3D shape matching, in: Proceedings of Eurographics/ACM SIGGRAPH Symposium on Geometry Processing, ACM, 2004, pp. 115–123.
12 A. Johnson, Surface landmark selection and matching in natural terrain, in: Proceedings of IEEE Conference on Computer Vision and Pattern Recognition, Vol. 2, 2000, pp. 413–420.
13 C. S. Chua, R. Jarvis, Point signatures: A new representation for 3D object recognition, International Journal of Computer Vision 25 (1) (1997) 63–85.
14 G. Tzimiropoulos, Project-out cascaded regression with an application to face alignment, in: Proceedings of IEEE Conference on Computer Vision and Pattern Recognition, 2015, pp. 3659–3667.
15 X. Cao, Y. Wei, F. Wen, J. Sun, Face alignment by explicit shape regression, International Journal of Computer Vision 107 (2) (2014) 177–190.
16 S. T. Gollmer, M. Kirschner, T. M. Buzug, S. Wesarg, Using image segmentation for evaluating 3D statistical shape models built with groupwise correspondence optimization, Computer Vision and Image Understanding 125 (2014) 283–303.
17 T. Baltrušaitis, P. Robinson, L.-P. Morency, 3D constrained local model for rigid and non-rigid facial tracking, in: Proceedings of IEEE Conference on Computer Vision and Pattern Recognition, 2012, pp. 2610–2617.
18 Y. Li, S. Wang, Y. Zhao, Q. Ji, Simultaneous facial feature tracking and facial expression recognition, IEEE Transactions on Image Processing 22 (7) (2013) 2559–2573.
19 J. M. Saragih, S. Lucey, J. F. Cohn, Deformable model fitting by regularized landmark mean-shift, International Journal of Computer Vision 91 (2) (2011) 200–215.
20 V. Le, J. Brandt, Z. Lin, L. Bourdev, T. Huang, Interactive facial feature localization, in: Proceedings of European Conference on Computer Vision, 2012, pp. 679–692.
21 P. Martins, R. Caseiro, J. Henriques, J. Batista, Discriminative bayesian active shape models, in: Proceedings of European Conference on Computer Vision, 2012, pp. 57–70.
22 P. Tresadern, P. Sauer, T. Cootes, Additive update predictors in active appearance models, in: Proceedings of British Machine Vision Conference, 2010, pp. 91.1–91.12.
23 H. Gao, H. K. Ekenel, M. Fischer, R. Stiefelhagen, Boosting pseudo census transform features for face alignment, in: Proceedings of British Machine Vision Conference, 2011, pp. 54.1–54.11.
24 I. Jolliffe, Principal Component Analysis, New York: Springer-Verlag, 2002.
25 Y. Tong, Y. Wang, Z. Zhu, Q. Ji, Robust facial feature tracking under varying face pose and facial expression, Pattern Recognition 40 (11) (2007) 3195–3208.
26 L. Liang, R. Xiao, F. Wen, J. Sun, Face alignment via component-based discriminative search, in: Proceedings of European Conference on Computer Vision, 2008, pp. 72–85.
27 Y. Nam, S. Hong, Real-time abnormal situation detection based on particle advection in crowded scenes, Journal of Real-Time Image Processing (2014) 1–14.
28 S. Ali, M. Shah, A lagrangian particle dynamics approach for crowd flow segmentation and stability analysis, in: Proceedings of IEEE Conference on Computer Vision and Pattern Recognition, 2007, pp. 1–6.
29 B. Solmaz, B. E. Moore, M. Shah, Identifying behaviors in crowd scenes using stability analysis for dynamical systems, IEEE Transactions on Pattern Analysis and Machine Intelligence 34 (10) (2012) 2064–2070.
30 M. De Berg, O. Cheong, M. Van Kreveld, M. Overmars, Computational Geometry: Algorithms and Applications, Springer-Verlag, 2008.
31 J. MacQueen, et al., Some methods for classification and analysis of multivariate observations, in: Proceedings of Berkeley symposium on mathematical statistics and probability, Vol. 1, 1967, pp. 281–297.
32 F. Bogo, J. Romero, M. Loper, M. J. Black, FAUST: Dataset and evaluation for 3D mesh registration, in: Proceedings of IEEE Conference on Computer Vision and Pattern Recognition, 2014.
33 P. Papadakis, The canonically posed 3D objects dataset, in: Proceedings of Eurographics Workshop on 3D Object Retrieval, 2014, pp. 33–36.
34 A. M. Bronstein, M. M. Bronstein, R. Kimmel, Numerical geometry of non-rigid shapes, Springer Science, 2008.